ELSEVIER

PALAEO

Palaeogeography, Palaeoclimatology, Palaeoecology 2795 (2002) 1–19

www.elsevier.com/locate/palaeo

Implications of Ordovician (≈460 Myr) marine cement for constraining seawater temperature and atmospheric pCO_2

Kenneth J. Tobin [a,*], Stig M. Bergstrom [b]

[a] *Department of Natural Sciences, Texas A&M International University, Laredo, TX 78041, USA*
[b] *Department of Geological Sciences, The Ohio State University, 155 S. Oval Mall, Columbus, OH 43210, USA*

Received 22 September 2000; received in revised form 22 June 2001; accepted 8 October 2001

Abstract

The marine diagenetic history of the Effna buildups (Virginia, lower Caradocian, ≈460 Myr) is atypical of Phanerozoic carbonates and reflects variable redox conditions in the semi-restricted Appalachian foreland basin. Fibrous marine cements are the focus of this study. Least-altered fibrous calcite from the Effna Formation has a translucent appearance in transmitted light and a 2–3 mol% $MgCO_3$ composition; the latter is similar to values (2–5 mol%) from translucent fibrous calcite in other Caradocian units [Holston (Tennessee) and Kullsberg (Sweden) formations]. Some fibrous calcite is overlain by hardgrounds that in places have an irregular micro-topography with sharp overhangs indicative of syn-depositional dissolution. Geochemical evidence supporting the marine dissolution includes $\delta^{18}O$ values from altered fibrous calcite that are more positive (up to −3.9‰ PDB) than coeval least-altered fibrous calcite from Holston buildups in Tennessee (up to −4.8 to −5.8‰ PDB). Syn-depositional dissolution was likely associated with sulfide oxidation along an oxic–anoxic interface and not due to upwelling of cold bottom water in the Appalachian foredeep. Faunal and lithologic evidence suggests that oxic surface waters had a normal salinity and a water temperature conducive for metazoan growth (< 33°C). This paper constrains the temperature of near-surface seawater in the Appalachian foreland basin (22–33°C) and atmospheric pCO_2 (> 14 present atmospheric level) during the early Caradocian. © 2002 Published by Elsevier Science B.V.

Keywords: Ordovician; marine cement; seawater temperature; atmospheric pCO_2

1. Introduction

Typically, the tacit assumption is generally made that the most-positive $\delta^{18}O$ value from ancient marine calcite reflects diagenetically least-altered material. This assumption is supported by the high degree of susceptibility to diagenetic alteration of marine $\delta^{18}O$ values. Diagenetic alteration associated with even a low water:rock ratio (< 10) can completely obliterate an original marine $\delta^{18}O$ signature (Banner and Hanson, 1990). This alteration is assumed to cause marine calcite $\delta^{18}O$ to be reset to more negative values. For example, in low-latitude settings, meteoric water has an $\delta^{18}O$ value that is 2–4‰ more negative than seawater (Dansgaard, 1964). Additionally, burial diagenetic alteration typically will also result in the resetting of marine $\delta^{18}O$ values to more negative values because of the decreased fractionation of oxygen isotopes between calcite and

* Corresponding author..
E-mail address: ktobin@tamiu.edu (K.J. Tobin).

0031-0182/02/$ – see front matter © 2002 Published by Elsevier Science B.V.
PII: S0031-0182(01)00436-9

water at elevated temperatures (Kim and O'Neil, 1997). However, alteration of marine material also is possible in undersaturated seawater. If the undersaturated seawater has a more positive $\delta^{18}O$ value (or lower temperature) than the original seawater from which a marine calcite was formed, then alteration can actually result in a product with a more positive $\delta^{18}O$ value relative to least-altered marine material.

Modern, shallow, low-latitude seawater is highly supersaturated (saturation index, SI = 0.8) with respect to calcite. However, recent modeling efforts indicate that the composition of ancient oceans and atmospheres were likely different than modern values. Hence, this paper assumes that the latest oceanic and atmospheric chemistry modeling efforts of Berner (1997), which constrains Phanerozoic atmospheric pCO_2, and Hardie (1996), which models how the major ion chemistry of seawater has varied throughout the Phanerozoic, provide more valid estimates of ancient atmospheric and oceanic chemistries. Parameters from these models can be used to estimate calcite SIs for ancient seawater.

This study focuses on marine calcite cements from the Ordovician Effna Formation in Virginia, which is $\approx$460 Ma (Cooper, 1999). The Effna Formation consists of organic (metazoan) buildups that were deposited in relatively shallow water (Read, 1982). Read (1982) discusses the presence of hardgrounds within the Effna buildups (his figures 6 and 7) and indicates that some of these hardgrounds have an irregular micro-topography with sharp overhangs indicative of syn-depositional dissolution (figure 12 from Read, 1982). This paper explores geochemical evidence that supports syn-depositional (marine) alteration of Effna marine cement. Additionally, on the basis of both geochemical and faunal evidence, this paper constrains the temperature and geochemistry of seawater within the Appalachian foreland basin during the early Caradocian and makes some inferences about atmospheric pCO_2 during this period.

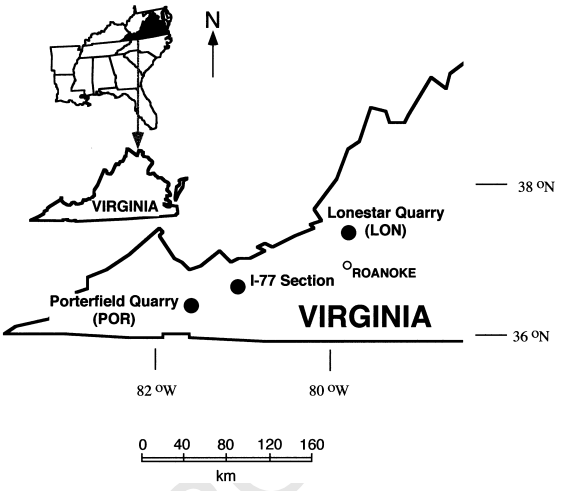

Fig. 1. Map showing location of POR, I-77 section, and LON localities.

2. Geologic setting, lithologies, and localities

The Effna Formation represents a series of downslope pinnacle buildups that were deposited along the western margin of the Appalachian foreland basin (Fig. 2). Read (1982) discusses in detail the nature and origin of these buildups, which extend upward for many tens of meters from a surrounding muddy slope to shallow shelf environment within the photic zone as indicated by the presence of algae in these buildups. These buildups were deposited during a period of rising relative sea level (Read, 1982), that ultimately resulted in their drowning with the deposition of the

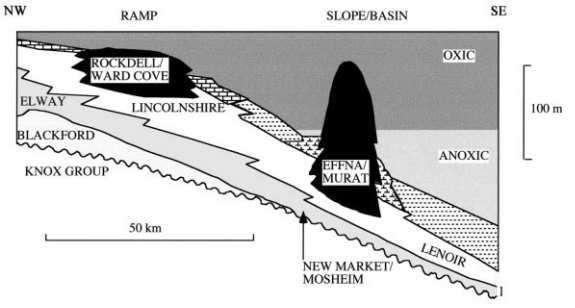

Fig. 2. Stratigraphic section of Middle Ordovician strata in southwestern Virginia that is approximately perpendicular to strike (cross section after Read, 1982). Names such as Effna, Lenior, etc., are formational-level units.

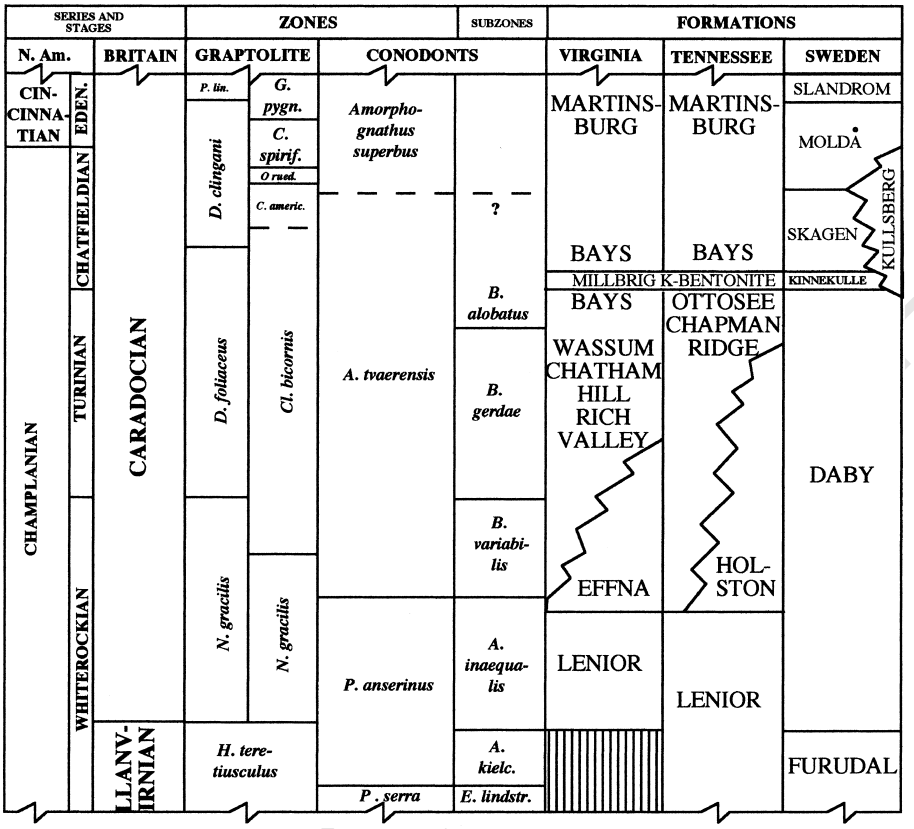

Fig. 3. Stratigraphic classification of the Effna Formation and other units referred to in text.

overlying deeper-water Liberty Hall Shale (Fig. 2). This part of the Middle Ordovician succession in southwestern Virginia represents a period of rapid thrust-induced subsidence due to the convergence of an island-arc system along the eastern Laurentian margin (Finney et al., 1996). Consequently, these deposits were never subaerially exposed early in their diagenetic history. Grover and Read (1983), in their seminal paper on cement stratigraphy, document the post-marine diagenetic history of these buildups, which consists of progressive burial with maximum burial depths (5–7 km) that were reached during the late Paleozoic.

The Effna buildups consist largely of coarse-grained echinoderm grainstones and 'muddy' wackestone/boundstone. Sampling at all localities concentrated in the wackestone/boundstone facies because of the dominance of fibrous calcite cement in this facies. Samples were collected from the Effna Formation at three localities in southwestern Virginia (Fig. 1). Geological details on locality information can be found in Grover (1981). The Interstate 77 (I-77) locality (Fig. 1) occurs along the northeast side of I-77 in southern Bland County, Virginia just north (<500 m) of Big Walker Mountain tunnel. Samples from I-77 and Lonestar Quarry (LON; Fig. 1) were collected near the crests of the buildup complex (see Read, 1982, his figure 7A). Conversely, the sampled biothermal deposits at the Porterfield Quarry (POR; Fig. 1) site were collected near the base of the buildup. Site access restrictions dictated sampling locations at LON and POR.

3. Biostratigraphy

In a study of this type, it is obviously important

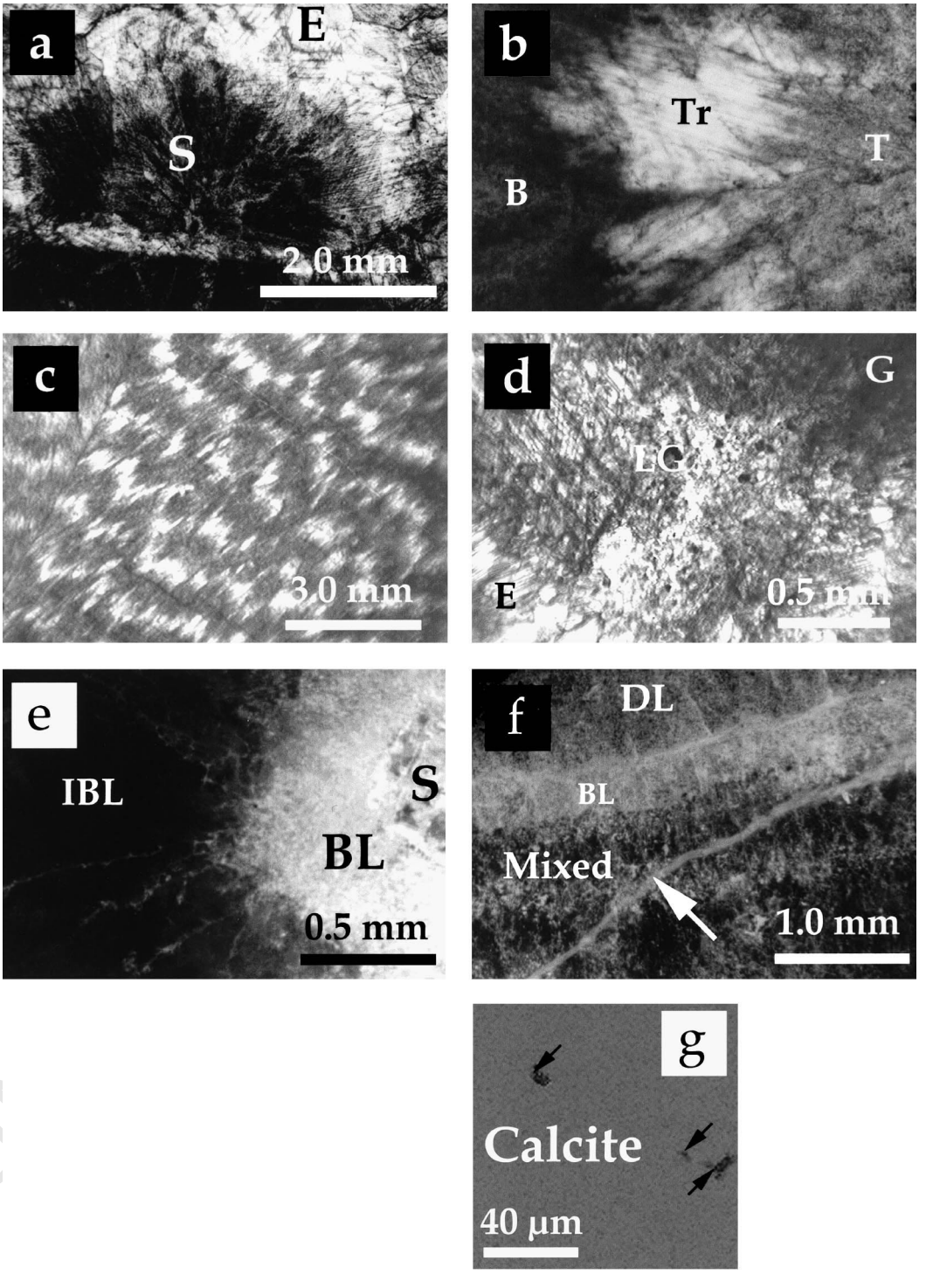

to have the geochemical information closely integrated with a precise biostratigraphic framework that will permit comparison with coeval units on a local and regional scale. Fortunately, the Effna Formation and adjacent strata are richly fossiliferous and these faunas include a variety of biostratigraphically diagnostic fossils. At the present time, conodonts provide the best biostratigraphic resolution in the case of these formations, and the many productive samples collected from these buildups permit placement of the Effna into standard Atlantic conodont zones and subzones. Bergström et al. (1988) showed the known vertical ranges of important conodont species through the Effna and adjacent units at the POR, and available information suggests that the biostratigraphical data from that section are valid for the Effna at other localities. Following Bergström et al. (1988), we correlate the base of the Effna with a level in the upper *P. anserinus* Conodont Zone a little below the base of the *A. tvaerensis* Zone. This level is coeval with a horizon in the middle of the *N. gracilis* Graptolite Zone and somewhat above the base of the British Caradocian Series and the base of the Baltic Kukrusean Stage. Because the base of this graptolite zone is now recommended to be the base of the global Upper Ordovician Series, the Effna is Late Ordovician in age in that classification although it would be Middle Ordovician (Champlainian) in terms of the traditional North American terminology (Ross et al., 1982). The Effna buildups vary significantly in height from locality to locality and hence, the age of the top of the formation is somewhat different at different localities. However, the conodont information available (Bergström et al., 1988) indicates that at all studied localities, the Effna does not range above the top of the *B. gerdae* Subzone of the *A. tvaerensis* Zone (Fig. 3). Based on the known relations between conodont and graptolite zones, the Effna is coeval with the upper part of the *N. gracilis* and lower part of the *D. foliaceus* (formerly *D. multidens*) Graptolite Zones. It is also broadly equivalent to the lower part of the Black River Group of New York. Within the biostratigraphic resolution now available, its base is at the same level as the base of the Holston Formation buildups of eastern Tennessee (Bergström and Carnes, 1976; Jaanusson and Bergström, 1980) but the top of the Holston, where the unit is particularly thick, may possibly be slightly younger than the top of the Effna although it is still within the *B. gerdae* Subzone. Importantly, both the Effna and the Holston are clearly older (early Caradocian) than the Kullsberg buildups in Sweden (middle Caradocian) but slightly younger than the Llandeilo buildups in the Chazy Group of Champlain Valley (Harris et al., 1979, their figure 16).

4. Methods

Petrographic thin sections (5×7.5 cm) were examined in detail in transmitted light. Staining of selected thin sections with potassium ferricyanide and Alizarin Red-S (method of Dickson, 1965, 1966) was used to identify dolomite and phases containing ferrous iron. Polished thin sections were studied using a Citl Cold Cathode Luminescence 8200 mk3 unit (voltage 10 kV, beam current 150–180 μA, and chamber pressure 180–200 mTorr) in order to discern homogeneous zones within cement phases that were large enough to

Fig. 4. Plane-polarized transmitted light photographs (except when noted) of calcite cements from the Effna Formation. (a) Brown turbid fibrous calcite with a spherulitic fabric (S) within cephalopod intragranular porosity that was subsequently completely occluded by equant calcite (E). (b) Translucent fibrous calcite (Tr) surrounded by gray turbid fibrous calcite (T) and brown turbid fibrous calcite (B). (c) Herringbone calcite with chevron-like pattern; compare with figure 3 in Sumner and Grotzinger (1996a,b). (d) Gray turbid fibrous calcite (G), light gray turbid fibrous calcite (LG), and pore-central equant calcite (E). (e) Cathodoluminescence photo. Fibrous calcite formed from a micritic substrate (S) with a band of bright luminescent (BL), turbid fibrous calcite and intrinsic blue luminescent (IBL), translucent fibrous calcite. (f) Cathodoluminescence photo. Brown-to-gray turbid fibrous calcite with highly variable luminescence (Mixed = mixed non-luminescent and dull luminescent; BL = bright luminescent; DL = mainly dull luminescent). White arrow points to cross-cutting vein. (g) Mg X-ray map showing the occurrence of microdolomite (arrows) in turbid fibrous calcite.

sample for isotopic analysis and to select areas for electron microprobe analysis.

Samples of cement for isotopic analysis were obtained by microdrilling areas on thin section billets, matched as closely as possible with accompanying thin sections. Resulting powders were roasted at 380°C for 1 h to remove organic contamination and then reacted off-line with 100% H_3PO_4 at 25°C for at least 12 h. Overall reproducibility is ±0.2‰ for $\delta^{13}C$ and $\delta^{18}O$ with results reported relative to PDB. Isotopic ratios were measured on a VG-903 isotope ratio mass spectrometer. Wavelength dispersive electron microprobe analysis for Mg, Ca, Mn, Fe, and Sr in calcite was performed on polished thin sections using a Cameca SX-50 Electron Microprobe (EMP). Operating conditions included an accelerating voltage of 25 kV, a beam current of 10 nA, and a defocused beam of 20 μm in width to minimize sample volatilization. Count times were as follows: Ca = 10 s; Mg = 20 s; Mn and Fe = 60 s; and Sr = 60 s with corresponding 2σ detection limits of Mg = 0.1 mol% $MgCO_3$; Mn and Fe = 100 ppm; and Sr = 200 ppm. In addition, the Mg distribution in selected fibrous calcite cements was observed with elemental X-ray map images. Analyses with high $MgCO_3$ content were screened with backscatter X-rays for the presence of microdolomite. Consequently, results reported reflect Mg concentration of calcite and not a mixture of calcite and dolomite at the micrometer to sub-micrometer scale.

5. Petrography of Effna marine cements

Grover (1981) defined three major types of marine cement (neospar, bladed, and turbid rim cement) in the Effna buildups. In this study, we focused mainly on neospar and bladed calcite cements as classified by Grover (1981). However, the classification of marine cements used in this paper differs from Grover (1981) in that it is nongenetic. We prefer to use the terms that describe crystal habit such as fibrous calcite (Folk, 1965) to terms like neospar. Petrographic evidence supporting a marine origin for fibrous calcite cement includes: (1) fibrous calcite interlayered with burrowed marine internal sediments (see Read, 1982); (2) cracks in fibrous cement are filled with marine internal sediment; (3) fibrous calcite fills stromatactis vugs, which are commonly interpreted as a marine diagenetic feature (Bathurst, 1980; Bourque and Boulvain, 1993, among others); and (4) compromise boundaries between fibrous calcite and turbid syntaxial overgrowths, interpreted as a marine precipitate (see Lohmann and Meyers, 1977; Walker et al., 1990), indicate contemporaneous precipitation of these phases.

Fibrous calcite is most abundant in 'muddy' wackestone/boundstone facies whereas turbid syntaxial overgrowths are dominant in coarse-grained, echinoderm grainstone facies. Fibrous calcite occurs as stromatactis and occludes intergranular, intragranular, moldic, and shelter voids. Fibrous calcite is mostly radiaxial fibrous with some fascicular-optic cement. Crystal boundaries are planar to highly jagged. Some fibrous calcite forms a spherulitic fabric (Fig. 4a).

Nearly all of the fibrous cement in the Effna buildups is turbid in appearance in plane polarized light. A small (< 300 μm) zone of translucent fibrous calcite (Fig. 4b) is present in one sample and is surrounded by turbid fibrous calcite. Turbid fibrous calcite can be subdivided based on its appearance, in descending order of abundance, into brown-to-gray turbid calcite (Fig. 4a, b, d), herringbone calcite (Sumner and Grotzinger, 1996a,b; Fig. 4c), and light gray turbid calcite (Fig. 4d). Brown-to-gray turbid fibrous calcite can consist of either discrete brown and gray turbid fibrous cement bands or conversely, gray cement can occur as irregularly shaped areas that are laterally gradational with brown cement.

At the POR locality some generalizations with regard to the relative timing of formation of the various turbid fibrous calcite subtypes can be made. Specifically, brown-to-gray turbid cement (or herringbone calcite) predates a major discontinuity surface that is overlain by micrite (Read, 1982, his figure 9b), pyrite/marcasite or iron oxide that is pseudomorphic after Fe-sulfides (Fig. 5), or micrite mixed with sulfides (or pseudomorphic iron oxide). Herringbone calcite (Sumner and Grotzinger, 1996a,b) is well developed only at POR and consists of chevron bands of dark

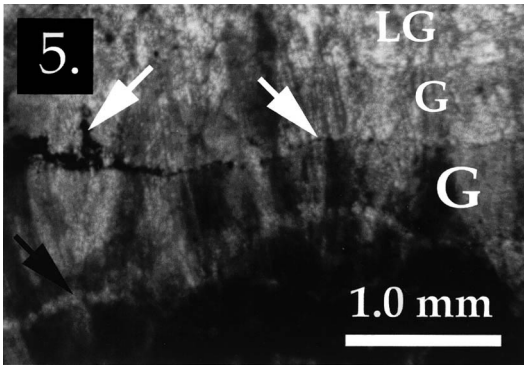

Fig. 5. Plane-polarized transmitted light photograph of layers of gray turbid fibrous calcite (G) separated by a discontinuity surface lined with opaque, iron oxide, which is pseudomorphic after pyrite and marcasite (arrows).

gray and light brown turbid fibrous calcite (Fig. 4c). The discontinuity surface is generally followed by gray (and/or light gray) turbid fibrous calcite. Light gray turbid fibrous calcite, when present, forms the final generation of fibrous calcite (Fig. 4d), which is post-dated by various burial carbonate cements (see Grover and Read, 1983).

The cathodoluminescence of fibrous calcite is quite variable. Rare, translucent fibrous calcite has a faint blue luminescent core with dully to brightly orange luminescent crystal edges (Fig. 4e). Brown turbid fibrous calcite is most commonly dully to moderately orange luminescent and gray turbid fibrous calcite is most commonly mixed non-luminescent and dully orange luminescent (Fig. 4f). Additionally, some gray turbid cement has faint blue luminescent crystal interiors with orange luminescent crystal rims like translucent fibrous calcite. Herringbone calcite is typically dully to moderately orange luminescent with darker appearing areas of this cement in transmitted light exhibiting the brighter luminescence. Light gray turbid fibrous calcite is moderately to brightly orange luminescent.

Inclusions are rare in translucent fibrous calcite, although minor fluid inclusions are present. Conversely, turbid fibrous calcite cements have an abundance of inclusions. Inclusions in turbid fibrous calcite are 1–50 μm in size and include microdolomite (Fig. 4g), fluid inclusions, pyrite/marcasite (and pseudomorphic iron oxides), and rounded to irregularly shaped, solid inclusions of unknown type. Disseminated iron oxide is particularly common in light gray turbid fibrous calcite. In most fibrous cements inclusions are uniformly distributed, but in some areas inclusion density is particularly high adjacent to crystal boundaries and cleavage traces.

6. Minor elemental and stable isotopic composition of Effna marine calcite

The $MgCO_3$ content of Effna fibrous calcite varies from 0.2 to 3.1 mol% (Fig. 6). The highest $MgCO_3$ concentrations, ranging from 1.8 to 3.1 mol%, are recorded from translucent fibrous cement that is intrinsically blue luminescent (Fig. 6). This cement has essentially no microdolomite (<0.1 vol.%, Fig. 6). Turbid fibrous cement has lower $MgCO_3$ concentrations that range from 0.2 to 1.4 mol% (Fig. 6). Abundance of microdolomite in turbid cement is variable (up to 5 vol.%, Figs. 4g, 6).

The Mn content of fibrous calcite varies from below the detection limit (100 ppm) to 3600 ppm. All analyses of translucent fibrous calcite are below the detection limit of 100 ppm (Fig. 6). Turbid fibrous calcite typically has more variable Mn values (brown-to-gray turbid = below detection limit to 3600 ppm; herringbone calcite = below detection limit to 600 ppm; light gray turbid = 200–500 ppm).

Most analyses for Fe of translucent fibrous calcite are below the detection limit (six out of eight) with a maximum value that is at the detection limit (100 ppm; Fig. 6). Turbid fibrous calcite has more variable, but still generally low, Fe concentrations (brown-to-gray = below detection limit to 1100 ppm; herringbone calcite = below detection limit to 300 ppm; light gray turbid = below detection limit). All fibrous calcite is non-ferroan as determined by KCN staining. Finally, all fibrous calcite has a Sr content near or below the detection limit (200 ppm).

Brown-to-gray turbid fibrous calcite ($n=36$) has $\delta^{13}C$ from -0.3 to $+1.0$‰ PDB and $\delta^{18}O$ from -3.9 to -7.9‰ PDB (Fig. 7). Herringbone

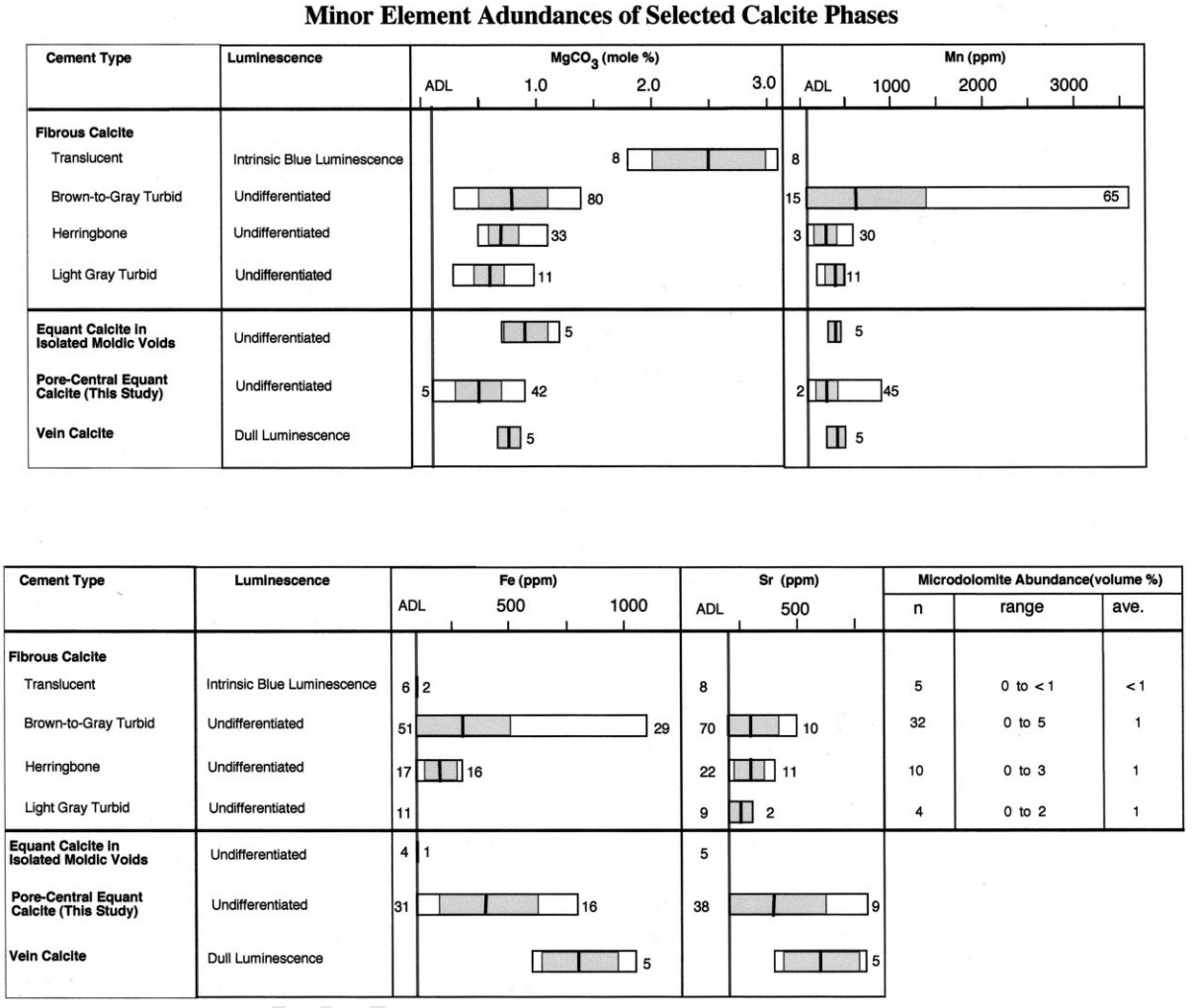

Fig. 6. Minor element compositions of calcite cement from the Effna Limestone. Gray vertical line shows analytical detection limit (ADL) which is 0.1 mol% for $MgCO_3$, 100 ppm for Mn and Fe, and 200 ppm for Sr. Black vertical lines represent mean composition and gray field is standard deviation of analyses including only analyses above detection limit. The wider unpatterned part of the bar shows the total range of values above detection limit. Numbers adjacent to horizontal bar represent number of analyses for a particular phase both below (to the left of gray vertical line) and at or above (to the right of gray vertical line) the detection limit. Additionally, microdolomite abundance based on X-ray mapping is shown for selected phases.

calcite ($n=12$) has a similar range of values ($\delta^{13}C=0$ to $+0.8‰$, $\delta^{18}O=-5.0$ to $-8.0‰$). Light gray turbid fibrous calcite ($n=6$) has $\delta^{13}C=-1.6$ to $+0.6‰$ and $\delta^{18}O=-5.7$ to $-8.0‰$. Equant calcite, which occludes pore-central porosity and post-dates fibrous calcite (Figs. 4d, 5), has similar $\delta^{13}C$ and partially overlaps in $\delta^{18}O$ values with fibrous calcite ($n=10$, $\delta^{13}C=+0.1$ to $+0.8‰$, $\delta^{18}O=-6.8$ to $-9.5‰$; Fig. 7).

7. Evidence for alteration of Effna turbid fibrous calcite

As mentioned above, extensive syn-depositional dissolution affected the Effna buildups (Read,

1982). Briefly, geochemical evidence supporting the extensively altered nature of turbid fibrous cements includes: (1) variable, but generally elevated (up to 5 vol.%), abundance of microdolomite (Fig. 4g); (2) highly variable cathodoluminescence (Fig. 4e, f); and (3) low calcite $MgCO_3$ concentrations (typically <1 mol%; Fig. 6) when compared with higher Mg concentrations in least-altered cement indicating stabilization from a higher Mg calcite precursor. EMP analyses of turbid marine cement that have elevated $MgCO_3$ values (>2 mol%) inevitably also have microdolomite inclusions within the crater formed during analysis. In addition, the stable isotopic composition of Effna turbid fibrous cements is variable (Fig. 7) and inconsistent with an unaltered marine isotopic signal, which is typically defined by a tight clustering of values (Tobin and Walker, 1997; Figs. 7, 8).

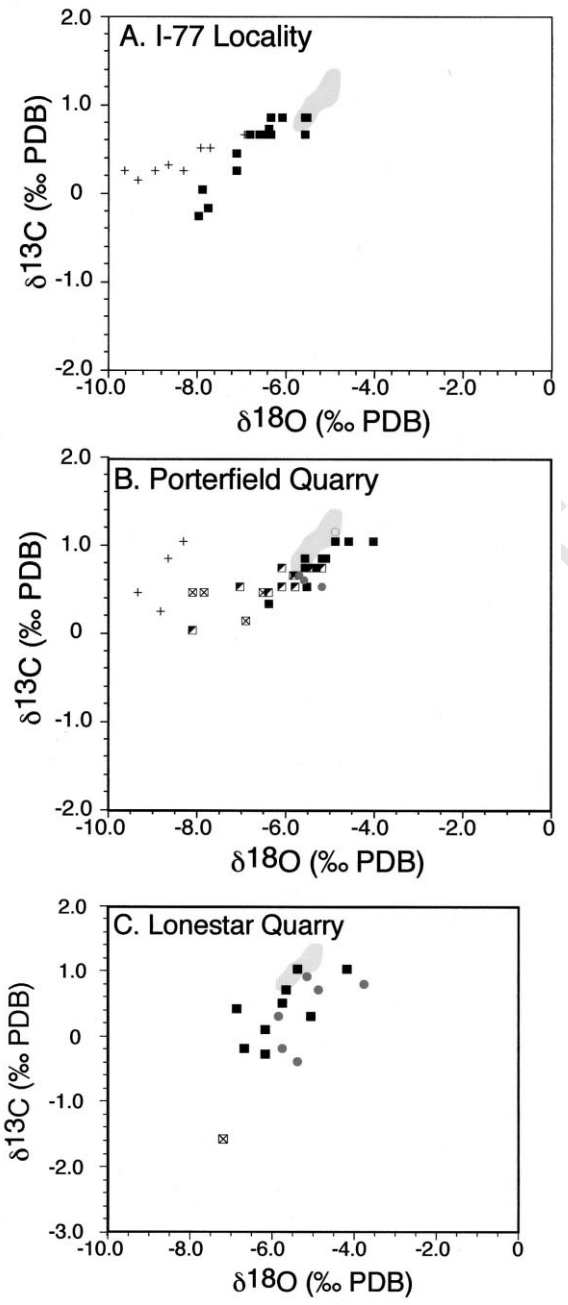

8. Least-altered, translucent fibrous calcite

The least diagenetically altered marine cement in the Effna Formation is translucent fibrous calcite, which is very rare and is briefly discussed below to provide a baseline for comparison with more altered fibrous cements. Carpenter and Lohmann (1989), Bourque and Raymond (1994), and Frank and Lohmann (1996) have previously recognized that translucent fibrous cement, from the Silurian to Holocene, is typically less altered when compared with turbid fibrous cement. Effna translucent fibrous cement has a $MgCO_3$ composition that ranges from 2 to 3 mol% (low-Mg calcite or LMC), which is higher than values from altered, turbid fibrous calcite. Additionally, there is essentially no microdolomite present in translucent fibrous calcite X-ray maps (<0.1 vol.%, $n=5$; Fig. 5). The $MgCO_3$ content of translucent fibrous calcite from other Caradocian units (Holston and Kullsberg formations), where this cement is also interpreted as a least-unaltered marine cement,

Fig. 7. $\delta^{13}C$ and $\delta^{18}O$ data from (A) I-77 section, (B) POR, and (C) LON. Data points from this study is black and from Grover (1981) gray. Fibrous calcite includes: undifferentiated (●); brown-to-gray turbid cement (■); herringbone calcite (◩); and light gray turbid cement (⊠). Turbid syntaxial overgrowths on echinoderms (○). Equant calcite pore-central equant calcite that post-dates fibrous calcite (+). Light gray field represents $\delta^{13}C$ and $\delta^{18}O$ data from Holston translucent fibrous calcite ($n=9$; Tobin and Walker, 1997; Tobin, unpublished data).

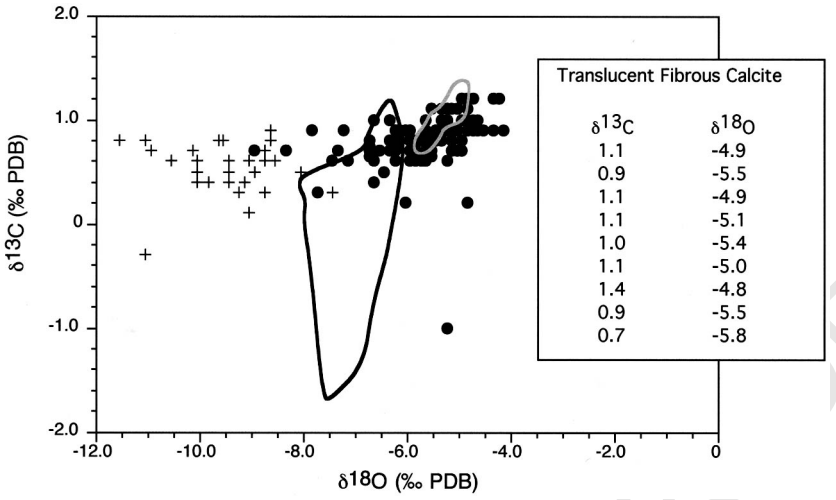

Fig. 8. Summary of $\delta^{13}C$ and $\delta^{18}O$ data from the Holston Formation (Steinhauff, 1993; Tobin and Walker, 1997). Turbid fibrous calcite (●) and various burial calcite phases (+). Black-outlined field reflects meteoric calcite values ($n=23$) from various Middle Ordovician units from northeastern Tennessee (Tobin et al., 1999) and gray-outlined field translucent fibrous calcite ($n=9$) from the Holston Formation (also see inset; Tobin and Walker, 1997; Tobin, unpublished data).

ranges from 2 to 5 mol% (Tobin and Walker, 1997). The small size of the translucent fibrous cement area present in the Effna Formation precludes conventional stable isotopic analysis. However, translucent fibrous calcite from the coeval Holston Formation in Tennessee exhibits a tight clustering of $\delta^{13}C$ and $\delta^{18}O$ values unlike turbid fibrous, meteoric, and burial calcite phases (Fig. 8). Least-altered fibrous calcite from Holston buildups has $\delta^{18}O=-4.8$ to -5.8‰ PDB ($n=9$; Tobin and Walker, 1997; Tobin, unpublished data; Fig. 8). The $\delta^{13}C$ and $\delta^{18}O$ values from the translucent fibrous calcite ($n=26$) of the Kullsberg Limestone in Sweden also exhibits a tight clustering (Tobin and Walker, 1997). All the lines of evidence discussed above suggest that translucent fibrous calcite has been minimally impacted by diagenesis and reflect a primary LMC precipitate, and therefore, can be used as a proxy for Caradocian seawater. Mackenzie and Pigott (1981) and Sandberg (1983) previously suggested that the Caradocian was a period of 'calcite' seas when LMC marine cements dominated unlike the 'aragonite' seas that typify shallow, warm, modern settings where aragonite and high-Mg calcite (HMC) are the dominant marine mineralogies.

9. Constraints on early Caradocian seawater temperature

Fossil faunas commonly provide important, and sometimes decisive, evidence concerning conditions in the depositional environment. The Effna Formation contains one of the most diverse macro- and microfossil faunas known in the Ordovician of the Appalachians, including close to 50 brachiopod species (Cooper, 1956), more than 20 trilobite species (Cooper, 1953), and numerous bryozoans, echinoderms, ostracodes, and conodonts. The great faunal diversity and great numbers of specimens, along with the presence of stenohaline taxas such as echinoderms, trilobites, and conodonts, suggest optimal paleoecological conditions, including normal seawater salinity and water temperatures <33°C as well as a high dissolved oxygen content.

An important piece of evidence regarding the water temperature in the depositional environment may be provided by the carbonate lithology in the successions containing the Effna and associated formations. Many of these limestones are of bahamitic type (Jaanusson and Bergström, 1980) that today are deposited at a minimum water temperature of about 22°C. Summarizing

the environmental evidence from the fossils and carbonate lithology just presented, it would appear that the Effna and associated units were deposited in seawater having a normal salinity and a temperature between 22 and 33°C.

Marine $\delta^{18}O$ values can be used constrain seawater temperature. Kim and O'Neil (1997) define the fractionation factor of oxygen isotopes between calcite and water as follows:

$$10^3 \ln \alpha_{\text{Calcite–H}_2\text{O}} = 2.78\ (10^6 T^{-2}) - 2.89 \qquad (1)$$

There is fundamental problem with the application of this expression. The fractionation factor incorporates both the calcite ($\delta^{18}O_{\text{Calcite}}$) and water ($\delta^{18}O_{H_2O}$) isotopic values as shown below:

$$10^3 \ln \alpha_{\text{Calcite–H2O}} \approx \Delta_{\text{Calcite–H2O}} =$$

$$\delta^{18}O_{\text{Calcite}} - \delta^{18}O_{\text{H2O}} \qquad (2)$$

Both temperature (T) and $\delta^{18}O_{H_2O}$ are unknowns. Water–rock interaction between seawater and mid-oceanic ridge suggest that the $\delta^{18}O$ value of seawater has remained fairly constant (-1 ± 2‰) throughout geologic time (e.g. Gregory, 1991) exclusive of the influence of variable global ice volume.

Read (1982) suggested that Effna marine cements formed from near-surface, oxic seawater. This assertion is supported by the intrinsic blue luminescence of translucent fibrous calcite from the Effna Formation, which is a characteristic that has been described in Iceland spar (Sippel and Glover, 1965). It is believed to be the intrinsic CL color of calcite and to be caused by the presence of lattice defects (Machel et al., 1991) in the absence of CL activators (e.g. Amieux et al., 1989). Concentrations of Mn and Fe in intrinsic blue luminescent, translucent fibrous cement are low when compared with all types of turbid fibrous calcite (Fig. 7). Additionally, this type of luminescence has also been observed in translucent fibrous calcite from other Ordovician units (Kullsberg and Holston formations), which are interpreted as examples of unaltered marine cement formed in an open-marine, oxic, diagenetic setting (Tobin and Walker, 1997).

Because the small size of Effna translucent fibrous cement precludes conventional stable isotopic analysis, translucent fibrous calcite from the Holston Formation is used as a proxy for near-surface, oxic seawater within the Appalachian foredeep. Deposition of the Holston buildups in Tennessee was coeval with that of the Effna buildup and took place in shallow water (≈ 50 m; Benedict and Walker, 1978; Walker, 1977, 1980). Note that Holston translucent fibrous cement has an average $MgCO_3$ concentration of 3 mol% (Tobin and Walker, 1997) and that the $\delta^{18}O$ value of calcite should be corrected for Mg content (Tarutani et al., 1969). The $\delta^{18}O$ value of calcite is increased by 0.06‰ for every 1 mol% $MgCO_3$ added to the calcite lattice, resulting in a 0.2‰ correction in this case. Corrected calcite $\delta^{18}O$ values are used with assumed seawater $\delta^{18}O$ values ranging from -3 to 1‰ SMOW to calculate the possible temperature of marine cements formation (Fig. 9). Within faunal temperature constraints of 22–33°C seawater $\delta^{18}O_{H_2O} = -2 \pm 1$‰ SMOW as previously indicated by Tobin and Walker (1997).

10. Constraints on early Caradocian atmosphere and seawater composition

10.1. Early Caradoc pCO_2 values

The only observational evidence for elevated Ordovician atmospheric pCO_2 (14 ± 6 present atmospheric level, PAL) comes from Yapp and Poths (1992) who examined goethitic paleosols from the latest Ordovician Neda Formation from the northern US midwest. It is not certain whether these paleosols correspond in age to the Hirnantian glaciation (≈ 438 Myr) episode near the end of the Ordovician or reflect ambient (non-glacial) greenhouse atmospheric pCO_2 levels before or after the glaciation(s). Berner (1991, 1994, 1997) also predicted elevated pCO_2 values for the early Caradocian (≈ 460 Myr) based on the results from his Phanerozoic carbon cycle modeling (8 to >25 PAL) with a best estimate of 21 PAL. Time steps for Berner's model are 10 Myr, and consequently, this model is insensitive to transient pCO_2 drawdown events like those

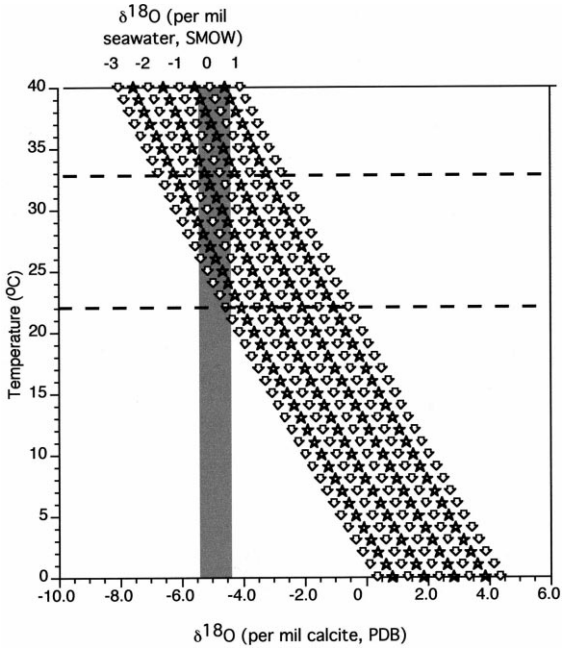

Fig. 9. Calculated paleotemperatures based on marine $\delta^{18}O$ values (gray rectangular field) from the Holston Formation using a range of seawater $\delta^{18}O$ compositions (1 to -3‰ SMOW). Dashed lines indicate faunal temperature constrains as discussed in the text.

that are interpreted to have happened during the middle Caradocian ($\approx$454 Myr; Ludvigson et al., 1996; Patzkowsky et al., 1997; Ainsaar et al., 1999; Meidla et al., 1999) and Hirnantian (Marshall and Middleton, 1990; Brenchley et al., 1994; Kump et al., 1999). Additionally, Gibbs et al. (1997) indicate that runaway glaciation would occur on an Ordovician earth if pCO_2 was <10 PAL. Elevated pCO_2 values for the Ordovician earth are required to offset the 4.5% decrease in solar luminosity present during this time period (Crowley and Baum, 1995). Consequently, Caradocian atmospheric pCO_2 was at least 10 PAL even during Hirnantian glaciation(s) and during ice-free periods of the Ordovician pCO_2 was likely higher (Gibbs et al., 1997).

10.2. Early Caradoc seawater composition

Today, the dominant kinetic inhibitor on modern marine calcite formation is the presence of Mg in seawater (Berner, 1975). However, if the Caradocian seawater had a Mg/Ca mole ratio = 1 (Wilkinson and Algeo, 1989; Hardie, 1996), then it is probable that Mg was not the dominant kinetic inhibitor preventing formation of Caradocian abiotic marine calcite. Indeed, experimental evidence presented by Fuchtbauer and Hardie (1976, 1980) indicates that when solution Mg/Ca mole ratio is less than 2, then LMC is the dominant abiotic carbonate precipitate from seawater and aragonite will not be observed, reflecting the lack of kinetic inhibition of Mg on calcite formation. Experimental results are consistent with our findings from Caradocian translucent fibrous calcite as discussed above.

Other kinetic inhibitors of calcite precipitation, besides Mg^{2+}, include PO_4^{3-}, SO_4^{2-}, and dissolved organic carbon (DOC). The link between PO_4^{3-} adsorption onto calcite (and aragonite) surfaces and the subsequent inhibition of calcite precipitation has been well established. As the calcite (and aragonite) SI approaches 0, Ca-carbonate precipitation rates are greatly impeded because of the increased effectiveness of surface adsorption of phosphate on to Ca-carbonate surfaces (Mucci, 1986; Burton and Walter, 1991). Sulfate has also been noted as a kinetic inhibitor of calcite precipitation (Mucci et al., 1989); however, its precise effect is highly variable depending on solution concentrations. For example, the presence of dissolved SO_4^{2-} in seawater greatly decreases the inhibitory effects of PO_4^{3-} on calcite precipitation (Burton, 1993). Experimental results given by Lebron and Suarez (1996) indicate that if DOC values are $\geq$0.5 mM then calcite formation will only occur above a minimum calcite SI value of 0.4. While the DOC of Caradocian seawater has not been modeled, some inferences can be made based on the widespread distribution of black shales during this time period (e.g. Leggett et al., 1981), which implies that the Caradocian ocean had elevated DOC values. Therefore, we suggest that a minimum calcite SI = 0.4 was necessary to facilitate the precipitation of Caradocian fibrous calcite.

Hardie, 1996 (his figure 3) modeled variations in major ion concentrations for Phanerozoic seawater. This quantitative model is based on steady-state mixing of hypothetical river water and mid-

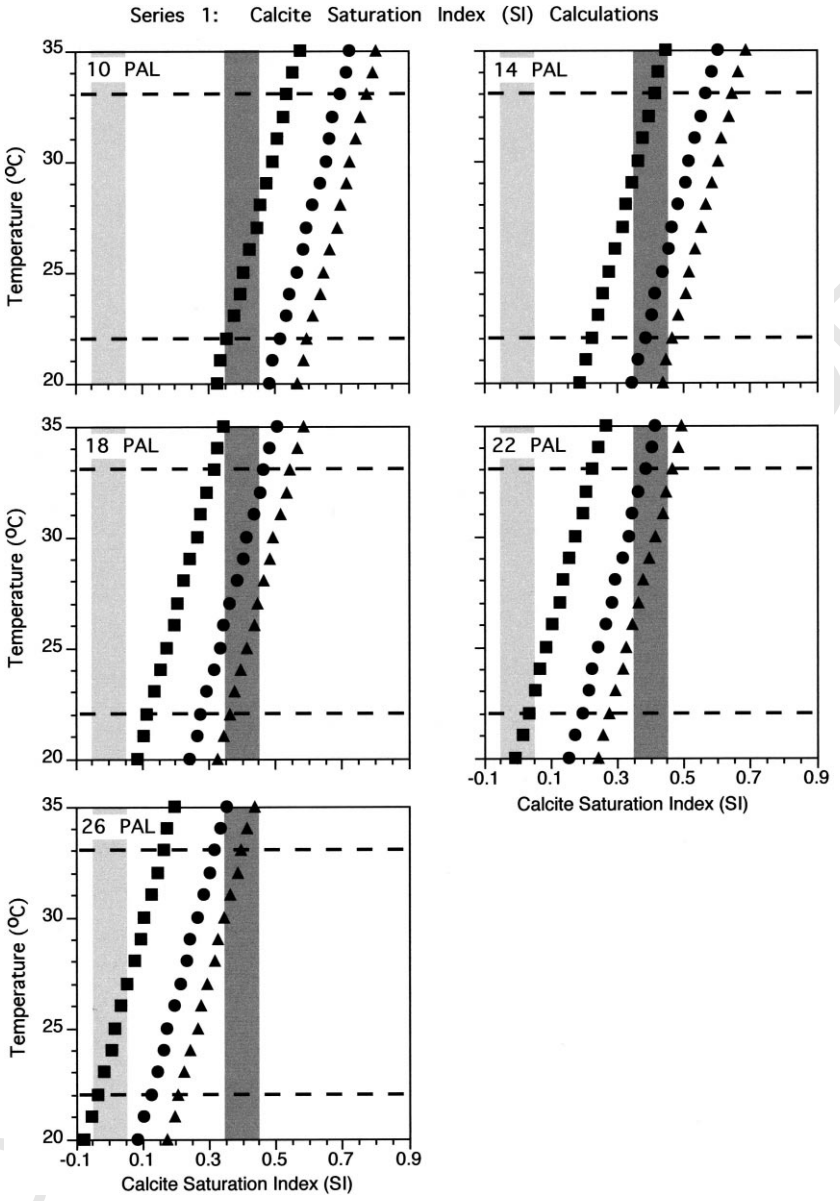

Fig. 10. Calcite saturation as determined by PHREEQC using early Caradocian seawater (Mg/Ca ratio = 1.25; ●) assuming a constant total alkalinity and differing atmospheric pCO_2 values. Additionally, Phanerozoic seawater that has a Mg/Ca ratio = 0.9 (▲) and 2.0 (■) are plotted. Dark gray field reflects minimum saturation needed to achieve abiotic marine calcite precipitation and light gray field defines seawater that is saturated with respect to calcite. Dashed lines indicate faunal temperature constrains as discussed in the text.

oceanic ridge hydrothermal brines (assumed mixing ratio 1.25). Modeled major ion concentrations, as well as assumed pCO_2 values, can be used to calculate the calcite SI of early Caradocian seawater for a range of temperatures using the computer program PHREEQC (Parkhurst and Appelo, 1999).

Two series of calculations were completed using modeled major ion concentrations. For series 1 calculations, three seawater compositions were

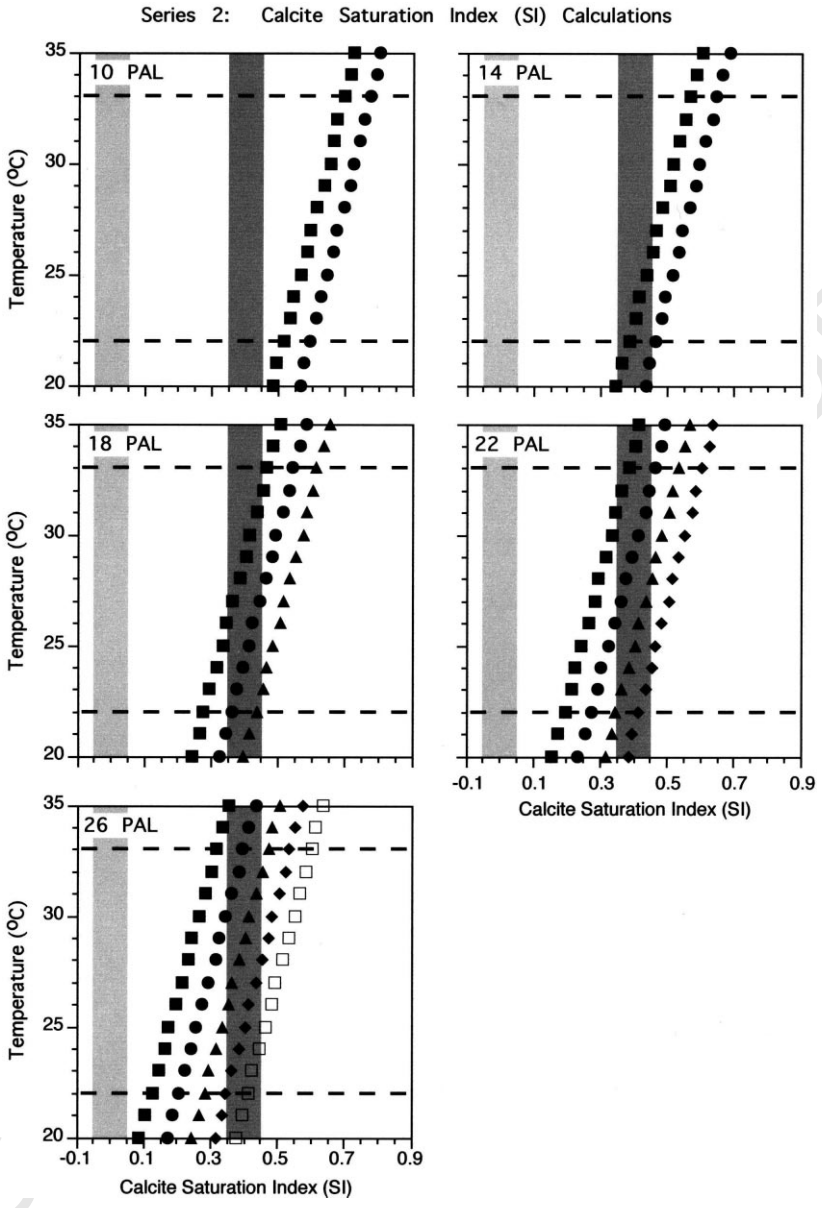

Fig. 11. Calcite saturation as determined by PHREEQC using early Caradocian seawater (Mg/Ca ratio = 1.25) and differing atmospheric pCO_2 values. Seawater with the modern value for total alkalinity is indicated by a square. Total alkalinity is increased by 10% increments above the modern value, which are depicted as follows (10%, ●; 20%, ▲; 30%, ◆; 40%, □). Dark gray field reflects minimum saturation needed to achieve abiotic marine calcite precipitation and light gray field defines seawater that is saturated with respect to calcite. Dashed lines indicate faunal temperature constrains as discussed in the text.

utilized to encompass the possible range of Mg/Ca ratios (Table 1). These compositions include a Phanerozoic minimum (Mg/Ca = 0.94), early Caradoc (Mg/Ca = 1.26), and maximum value when LMC is favored over HMC/aragonite (Mg/Ca = 2.00). Implicit to series 1 calculations (Fig. 10) is that the total alkalinity of seawater is constant at the modern value (2.41 mEq/kg; Morse and Mackenzie, 1990) no matter the pCO_2 value. The increase in carbonate alkalinity

($A_C = mHCO_3^- + mCO_3^{2-}$) resulting from elevated pCO_2 is offset by an increase in mH^+, which lowers seawater pH and maintains a constant total alkalinity. Decreased ancient seawater pH is not unprecedented; during the last 21 Myr pH has linearly increased from 7.4 to 8.2 based on boron isotope studies of foraminifers (Spivack et al., 1993). When seawater is assumed to have a Mg/Ca = 2.00 then a calcite SI value of 0.4, which we assume to be a minimum value needed for calcite precipitation, is reached only when $pCO_2 < 14$ PAL (Fig. 10). However, if assumed Mg/Ca ratio = 0.94 then calcite can form when pCO_2 is as high as 26 PAL (Fig. 10). Assuming that the early Caradocian Mg/Ca ratio = 1.26 then the calcite SI will equal 0.4 when $pCO_2 = 14$–22 PAL and $T = 22$–33°C (Fig. 10); results that are most similar to previous isotopic and carbon modeling studies as discussed above.

Series 2 calculations assume that the early Caradocian Mg/Ca ratio (1.26) is constant and in this series of calculations the total alkalinity is varied. The Ordovician is a period of overall greenhouse climate (Fischer, 1982) largely lacking continental ice sheets, except for the Hirnantian period (e.g. Brenchley et al., 1994). Consequently, there was likely an intensification of thermal transport to the poles resulting in an overall increase chemical weathering and erosion rates on land during this period. The net result is an increase in oceanic alkalinity derived from continental weathering. Consequently, we suggest that the total alkalinity of the Ordovician ocean was at least, if not greater than, the modern value. Series 2 calculations use the modern total alkalinity as a baseline with elevated alkalinity inputted at 10% increments (Fig. 11). The net affect of increased alkalinity is to increase calcite SI (Fig. 11). At a relatively low pCO_2 concentration of 14 PAL, calcite SI = 0.4 is achieved using the modern, baseline total alkalinity value. However, at elevated pCO_2 values ($pCO_2 > 22$ PAL) alkalinity must be adjusted upwards to keep calcite SI near the 0.4 threshold value for calcite precipitation (Fig. 11). Consequently, Ordovician pCO_2 was most likely to be between 14 and 22 PAL with higher pCO_2 values permissible with increased oceanic alkalinity.

11. Early Caradocian seawater $\delta^{18}O$ versus salinity

Since appropriate fluid inclusions were not present in the examined Effna and Holston marine cements, there is significant uncertainty in terms of how seawater $\delta^{18}O$ relates to salinity (S) during the early Caradocian. However, we can use as an approximation the parameters from the model of Railsback et al. (1989, 1990). Specifically, in modern oceans the relationship between seawater $\delta^{18}O-S$ defines two line segments. Slight modification of the modern relationship is necessary to account for the presumed ice-free nature of the early Caradocian earth resulting in the definition of the following two line segments representing: (1) the mixing of fresh and sea water when $S = 0$–34‰ and (2) the influence of evaporation at $S > 34$‰. Railsback et al. (1989) delimits the line segments with the following equations:

$$\delta^{18}O = \delta\,^{18}Oo + [(\Delta fw/So)\quad (S-So)]$$

$$for\quad S = 0 - 34‰\quad or \tag{3}$$

$$\delta^{18}O = \delta\,^{18}Oo + me\quad (S-So)\quad for\quad S > 34‰ \tag{4}$$

where So (34‰; Railsback et al., 1990) defines the point between the two line segments, which assumes seawater at global average salinity equals

Table 1
Modeled Phanerozoic major ion compositions from Hardie (1996)

	Mg^{2+} (mM)	K^+ (mM)	Ca^{2+} (mM)	SO_4^{2-} (mM)	Mg/Ca ratio
Phanerozoic minimum	44	41	47	24	0.94
Early Caradoc	48	35	38	25	1.26
Maximum value for LMC	52	17	26	28	2.00

the average global $\delta^{18}O$ value ($\delta^{18}Oo$; Railsback et al., 1989, 1990), which is assumed to be $-2‰$ SMOW. The parameter (Δfw) indicates the global difference in $\delta^{18}O$ between meteoric precipitation and seawater, which Railsback et al. (1989, 1990) assumes to be $8‰$. Finally, the parameter me defines the relationship between seawater $\delta^{18}O$ and S when $S > 34‰$. In modern restricted basins like the Red Sea and the Mediterranean, which have high S, me = 0.35 (Railsback et al., 1989, 1990).

12. Effna marine cement and foredeep seawater

Read (1982) discussed the presence of sulfide and phosphorite crusts that cap hardgrounds associated with the Effna buildups (his figure 12) as well as discontinuity surfaces between different layers of fibrous calcite (his figure 9; Fig. 5). Sulfide and phosphorite crusts predate burial diagenetic phases as discussed by Grover and Read (1983). Formation of sulfide crusts were interpreted to be associated with anoxic bottom waters that periodically onlapped on to the Effna buildups (Read, 1982). Presence of anoxic bottom waters within the Appalachian foredeep of Virgina is supported by the presence of downslope black shales and lime mudstones of the overlying Liberty Hall Formation (Fig. 2). Additionally, the downslope flanking beds of the Botetourt Formation (Fig. 2) have an abundance of organic material and pyrite that were interpreted to be deposited below the oxic–anoxic interface (Read, 1982).

Supporting evidence for syn-depositional dissolution of Effna marine calcite is the non-ferroan composition of all turbid (altered) marine calcite (Fig. 6). Immediately above the oxic–anoxic interface, where marine calcite dissolution is inferred to have occurred (Read, 1982), a paucity of ferrous iron in seawater should have resulted in an alteration product that is non-ferroan. Clearly, the alteration history of Effna marine cement is more complex than a single phase of syn-depositional dissolution. Some turbid fibrous calcites have highly negative $\delta^{18}O$ values (-7 to $-8‰$ PDB; Fig. 7) that are similar to values observed from Tennessee meteoric calcite (Tobin et al., 1999; Fig. 8), and overlap with $\delta^{18}O$ values from Effna burial calcite (-6.8 to $-9.5‰$ PDB; $n = 10$; Fig. 7). Consequently, it is likely that secondary phase(s) of meteoric (and burial) alteration affected Effna (and Holston) marine calcite. However, the most positive $\delta^{18}O$ values from Effna turbid fibrous calcite are significantly more positive ($-3.9‰$ PDB; Figs. 7, 8) than least-altered Holston translucent fibrous calcite (-4.8 to $-5.8‰$; $n = 9$), which are interpreted as a proxy for oxic surface water. Consequently, we suggest that the most positive $\delta^{18}O$ values from Effna turbid fibrous calcite were imparted during the syn-depositional alteration of this cement.

Read (1982) suggested syn-depositional dissolution of Effna marine calcite is most likely associated with oxidization of hydrogen sulfide at the oxic–anoxic interface that separates oxic near-surface and anoxic bottom waters within the Appalachian foredeep. Alternatively, dissolution could be the result of low-temperature Appalachian foredeep bottom waters that upwelled and interacted with Effna marine calcite. To achieve minimum undersaturation necessary to facilitate dissolution of Effna marine calcite by Appalachian foredeep bottom water without sulfide oxidation, as determined by PHREEQC ($pCO_2 = 18$ PAL; Mg/Ca = 1.25; modern total alkalinity, see above discussion), cold bottom water is required (4–9°C). At these temperatures, calcite $\delta^{18}O$ paleothermometry indicates that highly negative $\delta^{18}OH_2O$ values (-5 to $-6‰$ SMOW) for Appalachian foredeep bottom water are needed to be consistent with observed most positive $\delta^{18}O$-Calcite value from Effna fibrous calcite. Calculated salinity (Eq. 3 and 4) is very low ($S = 17$–$21‰$) and bottom water ρ would be less than 1.020. Consequently, bottom water would be less dense than near-surface water and a stable water column could not have developed.

Therefore, due to the association of Effna buildup deposits with iron sulfide crusts, it is likely that localized oxidization of sulfides facilitated the syn-depositional dissolution of Effna marine calcite. Between $T = 22$ and 33°C a modest 1 mM of H_2S must be oxidized to cause calcite SI values for fall below 0 using seawater in equilib-

rium with atmospheric $pCO_2 = 18$ PAL. Alternatively, calcite dissolution could have been favored by aerobic oxidation of organic material. However, if bottom waters were supercharged with carbonate alkalinity due to organic decomposition degassing of CO_2 at the oxic–anoxic interface would have favored carbonate precipitation and not dissolution (Grotzinger and Knoll, 1995). Consequently, if bottom waters were enriched with carbonate alkalinity, additional oxidization of H_2S must be invoked to counteract supersaturation caused by CO_2 degassing.

13. Conclusions

(1) Most marine calcite cements in the Effna buildups are altered and have a turbid appearance. Primary LMC cement is very rare and has a characteristic translucent appearance. This cement has very low Mn and Fe concentrations, intrinsic blue luminescence, and is interpreted to have precipitated from oxic Ordovician seawater.

(2) Turbid fibrous calcite cements have been extensively altered by diagenesis based on the presence of microdolomite, highly variable cathodoluminescence, and low calcite $MgCO_3$ concentrations of these cements. Additionally, the stable isotopic composition of Effna turbid fibrous cements is highly variable, unlike translucent fibrous calcite, which exhibits a tight clustering of $\delta^{13}C$ and $\delta^{18}O$ values.

(3) Calcite $\delta^{18}O$ paleothermometry and faunal evidence constrains the temperature of near-surface seawater in the Appalachian foreland basin to between 22 and 33°C during Effna and Holston organic buildup formation. Additionally, atmospheric pCO_2 during the early Caradoc was mostly likely greater than 14 PAL.

(4) Syn-depositional dissolution of Effna marine calcite most likely was associated with sulfide oxidation along an oxic–anoxic interface present within the Appalachian foredeep. Upwelling of cold bottom water in the Appalachian foredeep is not a viable mechanism to explain the syn-depositional dissolution of Effna marine calcite.

14. Uncited references

Patzkowsky and Holland, 1993

Acknowledgements

This study has been funded by NSF Grant EAR-9315651 (to senior author) and grants from the Royal Physiographic Society, Sweden and the Ohio State University to the junior author. A. Patchen, K. Howard, C. Mora, K.R. Walker, and M. Bennett are thanked for their assistance.

References

Ainsaar, L., Meidla, T., Martma, T., 1999. Evidence for a widespread carbon isotopic event associated with late Middle Ordovician sedimentological and faunal changes in Estonia. Geol. Mag. 136, 49–62.

Amieux, P., Bernier, P., Dalongeville, R., de Medwecki, V., 1989. Cathodoluminescence of carbonate-cemented Holocene beachrock from the Togo coastline (West Africa): an approach to early diagenesis. Sediment. Geol. 65, 262–272.

Banner, J.L., Hanson, G.N., 1990. Calculation of simultaneous isotopic and trace element variations during water-rock interaction with applications to carbonate diagenesis. Geochim. Cosmochim. Acta 54, 3123–3137.

Bathurst, R.G.C., 1980. Stromatactis-origin related to submarine-cemented crusts in Paleozoic mud mounds. Geology 8, 131–134.

Benedict, G.L., Walker, K.R., 1978. Paleobathymetric analysis in Paleozoic sequences and its geodynamic significance. Am. J. Sci. 278, 579–607.

Bergström, S.M., Carnes, J., 1976. Conodont biostratigraphy and paleoecology of the Holston Formation (Middle Ordovician) and associated strata in Eastern Tennessee. In: Barnes, C.R. (Ed.), Conodont Paleoecology. Geological Association of Canada Special Publication 15, pp. 27–58.

Bergström, S.M., Carnes, J.B., Hall, J.C., Kurapkat, W., O'Neill, B.E., 1988. Conodont biostratigraphy of some Middle Ordovician stratotypes in the Southern and Central Appalachians. N. Y. State Mus. Bull. 462, 20–32.

Berner, R.A., 1975. The role of magnesium in the crystal growth of calcite and aragonite from seawater. Geochim. Cosmochim. Acta 39, 489–504.

Berner, R.A., 1991. Paleo pCO_2 and climate. Nature 359, 114.

Berner, R.A., 1994. GEOCARB II, A revised model of atmosphere CO_2 over Phanerozoic time. Am. J. Sci. 294, 56–91.

Berner, R.A., 1997. The rise of plants and their effect on weathering and atmospheric CO_2. Science 276, 544–546.

Bourque, P.-A., Boulvain, F., 1993. A model for the origin and

petrogenesis of the red stromatactis limestone of Paleozoic carbonate mounds. J. Sediment. Petrol. 63, 607–619.

Bourque, P.-A., Raymond, L., 1994. Diagenetic alteration of early marine cements of Upper Silurian stromatactis. Sedimentology 41, 255–269.

Brenchley, P.J., Marshall, J.D., Carden, G.A.F., Robertson, D.B.F., Long, D.G.F., Meidla, T., Hints, L., Anderson, T.F., 1994. Bathymetric and isotopic evidence for a short-lived Late Ordovician glaciation in a greenhouse period. Geology 22, 295–298.

Burton, E.A., 1993. Controls on marine carbonate cement mineralogy: review and reassessment. Chem. Geol. 105, 163–179.

Burton, E.A., Walter, L.M., 1991. The effects of pCO_2 and temperature on magnesium incorporation in calcite in sea water and $MgCl_2$-$CaCl_2$ solutions. Geochim. Cosmochim. Acta 55, 777–785.

Carpenter, S.J., Lohmann, K.C., 1989. $\delta^{18}O$ and $\delta\ ^{13}C$ variations in Late Devonian marine cements from the Golden Spike and Nevis Reefs, Alberta, Canada. J. Sediment. Petrol. 59, 792–814.

Cooper, B.N., 1953. Trilobites from the Lower Champlainian Formations of the Appalachian Valley. Geological Society of America Memoir 55, 69 pp.

Cooper, G.A., 1956. Chazyan and Related Brachiopods. Smithsonian Miscellaneous Collections, v. 127, 1245 pp.

Cooper, R.A., 1999. The Ordovician time scale; calibration of graptolite and conodont zones. Acta Univ. Carolinae Geol. 43, 1–4.

Crowley, T.J., Baum, S.K., 1995. Reconciling Late Ordovician (440 Ma) glaciation with very high (14X) CO_2 levels. J. Geophys. Res. 100, 1093–1103.

Dansgaard, W., 1964. Stable isotopes in precipitation. Tellus 16, 436–468.

Dickson, J.A.D., 1965. Modified staining technique for carbonates in thin section. Nature 205, 587.

Dickson, J.A.D., 1966. Carbonate identification and genesis as revealed by staining. J. Sediment. Petrol. 36, 491–505.

Finney, S.C., Grubb, B.J., Hatcher, R.D., Jr., 1996. Graphic correlation of Middle Ordovician graptolite shale, southern Appalachians: An approach for examining the subsidence and migration of a Taconic foreland basin. Geol. Soc. Am. Bull. 108, 355–371.

Fischer, A.G., 1982. Long-term climatic oscillations recorded in stratigraphy. In: Climate and Earth History. National Research Council, Washington, pp. 97–104.

Folk, R.L., 1965. Some aspects of recrystallization in ancient limestones. In: Pray, L.C., Murray, R.C. (Eds.), Dolomitization and Limestone Diagenesis. Society of Ecomonic Paleontologists and Mineralogists Special Publication 13, pp. 14–48.

Frank, T.D., Lohmann, K.C., 1996. Diagenesis of fibrous magnesian calcite marine cement: implications for the interpretation of $\delta^{13}C$ and $\delta^{18}O$ values of ancient equivalents. Geochim. Cosmochim. Acta 60, 2427–2436.

Fuchtbauer, H., Hardie, L.A., 1976. Experimentally determined homogeneous distribution coefficients for precipitated magnesian calcites: Application to marine carbonate cements. Geol. Soc. Am. Abstr. Programs 8, 877.

Fuchtbauer, H., Hardie, L.A., 1980. Comparison of experimental and natural magnesian calcite. International Society of Sedimentologists Meeting, Bochum, Germany, pp. 167–169.

Gibbs, M.T., Barron, E.J., Kump, L.R., 1997. An atmospheric pCO_2 threshold for glaciation in the Late Ordovician. Geology 25, 447–450.

Gregory, R.T., 1991. Oxygen isotope history of seawater revisited: timescales for boundary event changes in the oxygen isotopic composition of sea water. In: Taylor, H.P., Jr., O'Neil, J.R., Kaplan, I.R. (Eds.), Stable Isotopic Geochemistry: A Tribute to Samuel Epstein. Geochemical Society, Special Publication No. 3, pp. 65–76.

Grotzinger, J.P., Knoll, A.H., 1995. Anomalous carbonate precipitates: Is the Precambrian the key to the Permian. Palaios 10, 578–596.

Grover, G., 1981. Cement types and cementation patterns of Middle Ordovician ramp-to-basin carbonates, Virginia (Ph.D. Dissertation). Virginia Polytechnic Institute and State University, 219 pp.

Grover, G., Read, J.F., 1983. Paleoaquifer and deep burial related cements defined by regional cathodoluminescent pattern, Middle Ordovician carbonates, Virginia. Am. Assoc. Pet. Geol. Bull. 67, 1275–1303.

Hardie, L.A., 1996. Secular variation in seawater chemistry: an explanation for the coupled secular variation in the mineralogies of marine limestones and potash evaporites over the past 600 m.y. Geology 24, 279–283.

Harris, A.G., Bergström, S.M., Ethington, R.L., Ross, R.J., 1979. Aspects of Middle and Upper Ordovician Conodont Biostratigraphy of Carbonate Facies in Nevada and Southeast California and Comparison with some Appalachian Successions. Brigham Young University Studies, v. 26 (3), pp. 7–33.

Jaanusson, V., Bergström, S.M., 1980. Middle Ordovician Faunal Spatial Differentiation in Baltoscandia and the Appalachians. Alcheringa, v. 4, pp. 89–110.

Kim, S.-T., O'Neil, J.R., 1997. Equilibrium and nonequilibrium oxygen isotope effects in synthetic carbonates. Geochim. Cosmochim. Acta 61, 3461–3475.

Kump, K.R., Arthur, M.A., Patzkowsky, M.E., Gibbs, M.T., Pinkus, D.S., Sheehan, P.M., 1999. A weathering hypothesis for glaciation at high atmospheric pCO_2 during the Late Ordovician. Palaeogeogr. Palaeoclimatol. Palaeoecol. 152, 173–187.

Lebron, I., Suarez, D.L., 1996. Calcite nucleation and precipitation kinetics as affected by dissolved organic matter at 25°C and $pH > 7.5$. Geochim. Cosmochim. Acta 60, 2765–2776.

Leggett, J.K., Mckerrow, W.S., Cocks, L.R.M., Rickards, R.B., 1981. Periodicity in the early Palaeozoic marine realm. J. Geol. Soc. Lond. 138, 167–176.

Lohmann, K.C., Meyers, W.J., 1977. Microdolomite inclusions in cloudy prismatic calcites; a proposed criterion for former high-magnesium calcites. J. Sediment. Petrol. 47, 1078–1088.

Ludvigson, G.A., Jacobson, S.R., Witzke, B.J., Gonzalez, L.A., 1996. Carbonate component chemostratigraphy and depositional history of the Ordovician Decorah Formation, Upper Mississippi Valley. In: Witzke, B.J., Ludvigson, G.A., Day, J. (Eds.), Paleozoic Sequence Stratigraphy: Views from the North American Craton. Geological Society of America Special Paper 306, pp. 67–86.

Machel, H.-G., Mason, R., Mariano, A.N., Mucci, A., 1991. Causes and emission of luminescence in calcite and dolomite. In: Barker, C.E., Kopp, O.C. (Eds.), Luminescence Microscopy: Quantitative and Qualitative Aspects. Society of Economic Paleontologist and Mineralogists Short Course 25, pp. 9–25.

Mackenzie, F.T., Pigott, J.D., 1981. Tectonic controls of Phanerozoic sedimentary rock cycling. Geol. Soc. Lond. J. 138, 183–196.

Marshall, J.D., Middleton, P.D., 1990. Changes in marine isotopic composition and the late Ordovician glaciation. J. Geol. Soc. Lond. 147, 1–4.

Meidla, T., Ainsaar, L., Hints, L., Hints, O., Nolvak, J., 1999. The mid-Caradocian biotic and isotopic event in the Ordovician of the east Baltic. Acta Univ. Carolinae Geol. 43, 503–506.

Morse, J.W., Mackenzie, F.T., 1990. Geochemistry of Sedimentary Carbonates. Developments in Sedimentology, No. 12. Elsevier, New York, 707 pp.

Mucci, A., 1986. Growth kinetics and composition of magnesian calcite overgrowths precipitated from seawater: Quantitative influence of orthophosphate ions. Geochim. Cosmochim. Acta 60, 2427–2436.

Mucci, A., Canuel, R., Zhong, S., 1989. The solubility of calcite and aragonite in sulphate-free sea water and the seeded growth kinetics and composition of the precipitates at 25°C. Chem. Geol. 47, 217–233.

Parkhurst, D.L., Appelo, C.A.J., 1999. User's guide to PHREEQC (Version 2) – A computer program for speciation, batch-reaction, one dimensional transport, and inverse geochemical calculations. Water-Resources Investigations Report 99-4259. United States Geological Survey, 326 pp.

Patzkowsky, M.E., Holland, S.E., 1993. Biotic response to a Middle Ordovician paleoceanographic event in eastern North America. Geology 21, 619–622.

Railsback, L.B., Ackerly, S.C., Anderson, T.F., Cisne, J.L., 1990. Paleontological and isotope evidence for warm saline deep waters in Ordovician oceans. Nature 343, 156–159.

Railsback, L.B., Anderson, T.F., Ackerly, S.C., Cisne, J.L., 1989. Paleoceanographic modeling of temperature-salinity profiles from stable isotopic data. Paleoceanography 4, 585–591.

Read, J.F., 1982. Geometry, facies, and development of Middle Ordovician carbonate buildups, Virginia Appalachians. Am. Assoc. Pet. Geol. Bull. 66, 189–209.

Ross, R.J., Jr., and 23 co-authors, 1982. The Ordovician System in the United States. Correlation Chart and Explanatory Notes. International Union of Geological Sciences Publication 12, 73 pp.

Sandberg, P.A., 1983. An oscillating trend in Phanerozoic nonskeletal carbonate mineralogy. Nature 305, 19–22.

Sippel, R.F., Glover, E.D., 1965. Structures in carbonate rocks made visible by luminescence petrography. Science 150, 732–739.

Spivack, A.J., You, C.-F., Smith, H.J., 1993. Forminiferal boron isotope ratios as a proxy for surface ocean pH over the past 21 Myr. Nature 363, 149–151.

Steinhauff, D.M., 1993. Sequence Stratigraphy and Comparative Diagenesis of Middle Ordovician Shelf to Shelf-Edge Limestones, The Copper Creek Allochthon, East Tennessee. Ph.D. Dissertation, University of Tennessee, Knoxville, TN, 460 pp.

Sumner, D.Y., Grotzinger, J.P., 1996a. Were kinectics of Archean calcium carbonate precipitation related to oxygen concentration. Geology 24, 119–122.

Sumner, D.Y., Grotzinger, J.P., 1996b. Herringbone calcite: petrography and environmental significance. J. Sediment. Res. 66, 419–429.

Tarutani, T., Clayton, R.N., Mayeda, T.K., 1969. The effect of polymorphism and magnesium substitution on oxygen isotope fractionation between calcium carbonate and water. Geochim. Cosmochim. Acta 36, 1237–1253.

Tobin, K.J., Steinhauff, D.M., Walker, K.R., 1999. Ordovician meteoric carbon and oxygen values: implications for the latitudinal variations of ancient stable isotopic values. Palaeogeogr. Palaeoclimatol. Palaeoecol. 150, 331–342.

Tobin, K.J., Walker, K.R., 1997. Ordovician oxygen isotopes and paleotemperatures. Palaeogeogr. Palaeoclimatol. Palaeoecol. 129, 269–290.

Walker, K.R., 1977. A brief introduction to the ecostratigraphy of the Middle Ordovician of Tennessee (southern Appalachians, U.S.A.). In: Ruppel, S.C., Walker, K.R. (Eds.), The Ecostratigraphy of the Middle Ordovician of the Southern Appalachians (Kentucky, Tennessee, and Virginia), U.S.A. A Field Excursion. University of Tennessee, Knoxville, Department of Geological Sciences Studies in Geology 1, pp. 12–17.

Walker, K.R., 1980. Pure carbonate within shales mark rejuvenation of shelf edge along Alcoa Highway. In: Walker, K.R., Broadhead, T.W., Keller, F.B. (Eds.), Middle Ordovician Carbonate Shelf to Deep Water Basin Deposition in the Southern Appalachians: Field Trip 10. University of Tennessee Studies in Geology No. 4, 120 pp.

Walker, K.R., Jernigan, D.G., Weber, L.J., 1990. Petrographic criteria for the recognition of marine, syntaxial overgrowths and their distribution in geologic time. Carbonates Evaporites 5, 141–152.

Wilkinson, B.H., Algeo, T.J., 1989. Sedimentary carbonate record of calcium-magnesium cycling. Am. J. Sci. 289, 1158–1194.

Yapp, C.J., Poths, H., 1992. Ancient atmospheric CO_2 pressures inferred from natural goethites. Nature 355, 342–343.